



Enhanced piezoelectric performance of rare earth complex-doped sandwich-structured electrospun P(VDF-HFP) multifunctional composite nanofiber membranes

Guimao Fu¹, Yongqing He¹, Yongri Liang³, Shifeng He¹, Rui Xue¹, Yibo Wu¹, Weiyong Yu², and Qisong Shi^{1,*}

¹ Beijing Key Laboratory of Special Elastomeric Composite Materials, College of New Materials and Chemical Engineering, Beijing Institute of Petrochemical Technology, Beijing 102617, China

² Academy of Artificial Intelligence, Beijing Institute of Petrochemical Technology, Beijing 102617, China

³ State Key Laboratory of Metastable Materials Science and Technology, School of Materials Science and Engineering, Yanshan University, Hebei 066012, China

Received: 6 June 2022

Accepted: 26 August 2022

Published online:

9 September 2022

© The Author(s), under exclusive licence to Springer Science+Business Media, LLC, part of Springer Nature 2022

ABSTRACT

In this paper, the electrospinning of Polyvinylidene hexafluoropropylene (P(VDF-HFP)) composite nanofibers was performed by adding rare earth complexes $\text{Eu}(\text{TTA})_3(\text{TPPO})_2$ and $\text{FeCl}_3 \cdot 6\text{H}_2\text{O}$ as fillers. The effects of $\text{Eu}(\text{TTA})_3(\text{TPPO})_2$ and $\text{FeCl}_3 \cdot 6\text{H}_2\text{O}$ fillers on the morphology, crystal structure, thermal properties, and fluorescence properties of P(VDF-HFP) composite nanofibers were investigated by the scanning electron microscopy, Fourier transform infrared spectroscopy, atomic force microscopy, X-ray diffraction, and differential scanning calorimetry and fluorescence. The mechanical properties, sensitivity, ferroelectric properties, and piezoelectric output of monolayer and sandwich structure composite nanofiber membranes used as sensors were studied. The results show that the synergistic effect of double fillers increases the content of β -phase with piezoelectric properties by nearly 20%, reaching 96.9%. The sandwich structure of the PU/P(VDF-HFP)- $\text{Eu}(\text{TTA})_3(\text{TPPO})_2$ - $\text{FeCl}_3 \cdot 6\text{H}_2\text{O}$ /PU flexible sensor has high sensitivity ($\sim 0.29 \text{ kPa}^{-1}$), high piezoelectric output ($\sim 3.7 \text{ V}$), high strain ($\sim 230\%$), and fluorescence characteristics. It is expected to be applied in wearable flexible sensors, photoelectric devices, and other fields.

Address correspondence to E-mail: shiqisong@bipt.edu.cn

1 Introduction

In recent years, the application of piezoelectric materials has been expanding. Piezoelectric materials can produce electric field due to mechanical deformation or mechanical deformation due to electric field action [1, 2]. Traditional piezoelectric or ceramic materials have been widely used to collect energy from mechanical energy, but the low flexibility and high weight of such ceramics limit their application in different fields. Compared with inorganic materials, organic piezoelectric materials represented by Polyvinylidene fluoride (PVDF) and its polymers have high chemical stability, good bending and tensile properties, and have the advantages of piezoelectric, dielectric, thermoelectric, flexible, easy processing, etc., which are widely used in sensors, actuators, and energy storage applications [3–5].

PVDF and its polymers mainly have three crystal forms: α , β , and γ , among which α -crystals are the most stable thermodynamically and β -phase PVDF with a polar crystal structure can exhibit strong piezoelectricity and also shows better ferroelectric, thermoelectric, and dielectric properties [6]. However, PVDF is mainly composed of α -phase, so the key to improve the piezoelectric properties of PVDF material is to increase the content of β phase. At present, most of the researches mainly use various methods to increase β -crystal content, such as electrostatic spinning, mechanical drawing and adding polarity induction of nanoparticles. Among them, the nanofiber membrane prepared by electrospinning technology has the characteristics of large specific surface area, high porosity, easy control of size, and easy functionalization of the surface. At the same time, the polarization effect of the high electrostatic field and the high draw ratio during the electrospinning process are similar to uniaxial mechanical stretching can cause β -phase transformation [7–9]. In addition, the addition of filler particles can induce the formation of β -phase crystals in the composite film, thereby achieving the purpose of enhancing the piezoelectric performance [10]. A large number of studies have shown that by adding rare earth ions (RE^{3+}) into the polymer nanofibers, the electronic and structural properties of the nanofibers can be changed, and the transformation of α - to β -phase in PVDF can be promoted, thus further improving its piezoelectric properties [11–13]. Moreover, the interaction between RE^{3+} ions and surrounding molecules will

affect the spectral characteristics of the system [14], thus greatly expanding the application range of functional nanofibers.

Adhikary et al. used Eu^{3+} -doped P(VDF-HFP) to prepare hybrid nanocomposite films with high-voltage electrical properties for the preparation of ultra-sensitive wearable piezoelectric nanogenerators (WPNGs) [15]. Li et al. used ferric chloride as oxidant, and PVDF nanofibers with high proportion were prepared by electrospinning β -phase PVDF nanofibers and PVDF beads [16]. In addition, mixed spinning and superimposed spinning are conducive to the improvement of nanofiber film morphology and mechanical properties. Among them, the composite film obtained by superimposed spinning is thinner [2, 17, 18]. Andreas Greiner and Markus Retsch et al. used porous thermoplastic polyurethane (TPU) as a flexible substrate and silver nanowires (AgNWs) as a conductive network system to easily realize a “sandwich” composite conductive material with both high flexibility and low resistance [19]. The development of multifunctional composite piezoelectric materials is of great significance in many applications in future. However, there are few reports on integrating multiple functions. Therefore, the development of a high-performance, multifunctional piezoelectric material is our research direction.

In this paper, a high performance and multifunctional sandwich piezoelectric nanofiber membrane was prepared by layer by layer spinning, which was enhanced by doping Eu^{3+} electrospinning P(VDF-HFP)/ $FeCl_3 \cdot 6H_2O$ nanocomposite. The doping addition further reduces the fiber diameter and enhances the piezoelectricity. The content of β -phase increased by nearly 20–96.9%. The sensitivity of the sandwich structure nanofiber membrane was increased 3.6 times. The strain can reach 230%, and it also has certain fluorescence characteristics. In this work, multifunctional piezoelectric nanofiber materials have been successfully prepared, which is expected to be applied in the fields of wearable electronics, intelligent sensors, and optoelectronic devices.

2 Experimental

2.1 Materials

Polyvinylidene fluoride hexafluoropropylene (P(VDF-HFP), $M_w = 400,000$), Sigma-Aldrich

(Shanghai) Trading Co., Ltd, Iron(III) Chloride Hexahydrate ($\text{FeCl}_3 \cdot 6\text{H}_2\text{O}$) Shanghai Titan Scientific Co., Ltd., and tetrahydrofuran (THF) and N,N-Dimethylformamide (DMF) were all obtained from Shanghai Titan Scientific Co., Ltd. Acetone (Ac) was purchased from Beijing Chemical Works. 2-thienylformyltrifluoroacetone (TTA), triphenylphosphine oxide (TPPO), and europium nitrate hexahydrate ($\text{Eu}(\text{NO}_3)_3 \cdot 6\text{H}_2\text{O}$) from Beijing J & K SCIENTIFIC LTD.

2.2 Preparation of P(VDF-HFP) composite nanofibers

P(VDF-HFP) was dissolved in the mixed solvent of DMF and Ac at 60 °C and stirred for 3 h and then a certain amount of Eu complex (recorded as C: prepared by the method we reported previously [20]) and $\text{FeCl}_3 \cdot 6\text{H}_2\text{O}$ (recorded as Fe) were added and stirred for 12 h to obtain electrospinning solution. At room temperature and $40 \pm 5\%$ humidity, 2 ml spinning solution was extracted with the needle of inner diameter 0.4 mm, a feed rate of 1 ml/h, and the voltage of 21 kV to prepare composite nanofiber membrane. The receiving distance between the needle tip and the collector is 15 cm. The fiber was collected by an aluminum roller drum. The nanofiber films obtained from the control experiment and doping C, Fe and the mixture of C and Fe were recorded as PFP, PFPC, PFPFe, and PFPCFe, respectively, as detailed in Table 1. At the same time, the prepared PU spinning solution dissolved in the mixed solvent of DMF and THF was spun layer by layer on the upper and lower surfaces of PFP, PFPC, PFPFe, and PFPCFe fiber membranes to prepare sandwich-structured membrane, which were recorded as PU/PFP/PU, PU/PFPC/PU, PU/PFPFe/PU, and PU/PFPCFe/PU, respectively.

2.3 Characterizations

The fiber morphology was observed by COXEM EM 30 PLUS high-precision secondary electron detector and EDS analysis was carried out with Oxford

X-max. Each fiber size distribution was calculated from each SEM images using the measurement tool in ImageJ software. FTIR-850 Fourier transform infrared spectrometer was used to test the fiber film. Photoluminescence spectra were obtained on FS5 fluorescence spectrometer. The X-ray diffraction (XRD) spectra of the samples were measured by XRD-7000 X-ray diffractometer, scanning range of 2θ from 5° to 30° , stride length of 0.02° , and scanning rate of $1^\circ/\text{min}$. The AFM test was obtained by MFP-3D Origin (Oxford Instruments Co., USA). DSC and TG curves were obtained by Setline thermogravimetric analyzer (TGA) at a rate of $10^\circ\text{C}/\text{min}$ from room temperature to 800°C . The tensile strength of film was tested by High-Temperature Tensile Testing Machine GP6220 of Suzhou Gaopin Testing Instrument Co., Ltd. The sensitivity of the packaged sensor was tested by the TH2828 Precision LCR Meter Digital Bridge Instrument and the ferroelectric properties of the composite nanofibers were studied using the TF2000E Ferroelectric Analyzer. We used home-made pressure equipment which could exert periodic impact force. Picoammeter (Keithley 6487) and digital oscilloscope (GDS-2102) were used to record piezoelectric current and voltage. All measurements were carried out at room temperature.

3 Results and discussion

3.1 Characterization of fluorescent complexes $\text{Eu}(\text{TTA})_3(\text{TPPO})_2$

Figure 1a is the infrared spectrum of fluorescent complex $\text{Eu}(\text{TTA})_3(\text{TPPO})_2$ (C). It can be found that the peak of the complex is concentrated in $2000\text{--}600\text{ cm}^{-1}$, the vibration absorption peak of benzene ring is at 1606 cm^{-1} , and the out-of-plane bending of benzene ring C–H is at $900\text{--}690\text{ cm}^{-1}$. The obvious absorption peak at about 740 cm^{-1} indicated that the coordination of Eu and O was successful, which proved that the synthesis of fluorescent complex $\text{Eu}(\text{TTA})_3(\text{TPPO})_2$ was successful.

Table 1 $\text{Eu}(\text{TTA})_3(\text{TPPO})_2/\text{FeCl}_3 \cdot 6\text{H}_2\text{O}$ system experimental formulation

Sample	P(VDF-HFP)/g	(DMF + Ac)/ml	$\text{Eu}(\text{TTA})_3(\text{TPPO})_2/\text{g}$	$\text{FeCl}_3 \cdot 6\text{H}_2\text{O}/\text{g}$
PFP	1.5	4 + 2	0	0
PFPC	1.5	4 + 2	0.15	0
PFPFe	1.5	4 + 2	0	0.02
PFPCFe	1.5	4 + 2	0.15	0.02

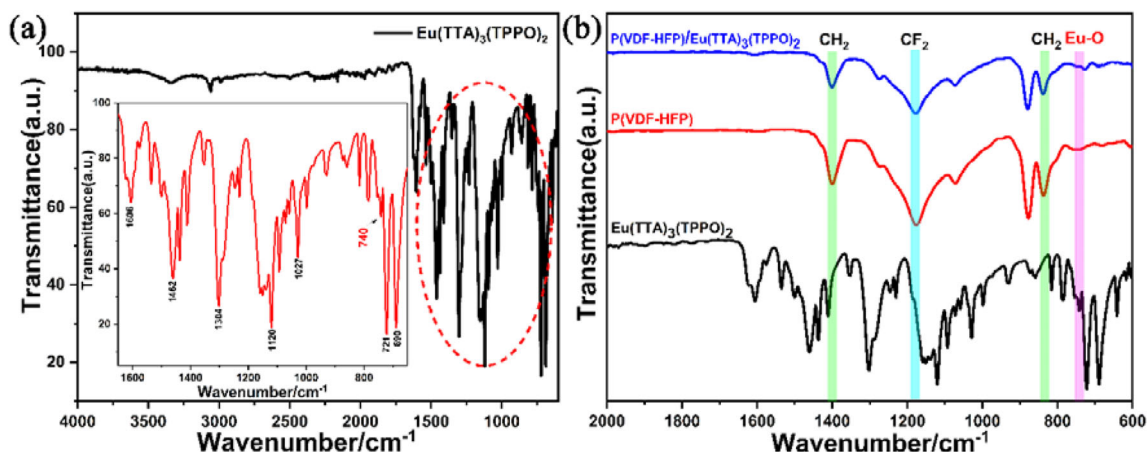


Fig. 1 FTIR spectra for **a** the complex $\text{Eu}(\text{TTA})_3(\text{TPPO})_2$, **b** comparison of $\text{Eu}(\text{TTA})_3(\text{TPPO})_2$, $\text{P}(\text{VDF-HFP})$, and $\text{P}(\text{VDF-HFP})/\text{Eu}(\text{TTA})_3(\text{TPPO})_2$

FT-IR (Fig. 1b) showed that $\text{P}(\text{VDF-HFP})$ characteristic peaks were found at 1400 cm^{-1} and 1185 cm^{-1} , corresponding to asymmetric vibration absorption peaks of CH_2 and bending vibration and stretching vibration absorption peaks of CF_2 , respectively. The absorption band at 840 cm^{-1} is the characteristic absorption band of amorphous β -phase. After doping, the characteristic peaks of $\text{Eu}(\text{TTA})_3(\text{TPPO})_2$ and $\text{P}(\text{VDF-HFP})$ moved to high frequency slightly. This indicated that the complex $\text{Eu}(\text{TTA})_3(\text{TPPO})_2$ was effectively integrated into the $\text{P}(\text{VDF-HFP})$ polymer matrix and its vibration frequency changed.

Fluorescence experiments were carried out on the complex $\text{Eu}(\text{TTA})_3(\text{TPPO})_2$. The excitation spectra were obtained by fixing the emission wavelength at 617 nm , and the absorption peak at 298 nm was the best. The emission spectrum in Fig. 2 shows that the

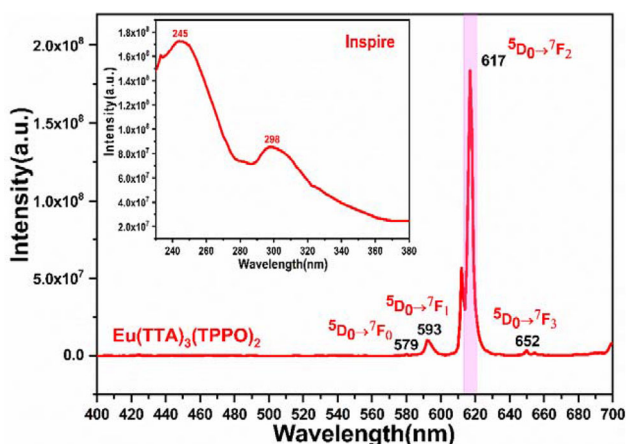


Fig. 2 Complexes $\text{Eu}(\text{TTA})_3(\text{TPPO})_2$ excitation and emission diagrams

decibel of the emission peak at $579, 593, 617,$ and 652 nm corresponds to the ${}^5\text{D}_0 \rightarrow {}^7\text{F}_0, {}^5\text{D}_0 \rightarrow {}^7\text{F}_1, {}^5\text{D}_0 \rightarrow {}^7\text{F}_2,$ and ${}^5\text{D}_0 \rightarrow {}^7\text{F}_3$ transition of Eu^{3+} , wherein the ${}^5\text{D}_0 \rightarrow {}^7\text{F}_2$ transition is the strongest emission peak, followed by ${}^5\text{D}_0 \rightarrow {}^7\text{F}_1$ transition. At the same time, the prepared complex powder can emit Eu^{3+} characteristic red fluorescence under UV light, which further confirms that the preparation of $\text{Eu}(\text{TTA})_3(\text{TPPO})_2$ is successful. Further, the PFPCFe nanofibers were prepared by doping the polymer matrix $\text{P}(\text{VDF-HFP})$, fluorescence complex $\text{Eu}(\text{TTA})_3(\text{TPPO})_2$, and filler $\text{FeCl}_3 \cdot 6\text{H}_2\text{O}$.

Figure 3 shows the presence of C, O, Eu, P, S, F, Cl, and Fe elements in PFPCFe fiber, which not only confirms that the complex $\text{Eu}(\text{TTA})_3(\text{TPPO})_2$ has been successfully prepared but also indicates that it is successfully integrated into $\text{P}(\text{VDF-HFP})$ polymer matrix with $\text{FeCl}_3 \cdot 6\text{H}_2\text{O}$. At the same time, the uniform distribution of Eu and Fe elements in Fig. 5 also confirms this.

In addition, thermal properties of the complex $\text{Eu}(\text{TTA})_3(\text{TPPO})_2$ were also analyzed. Figure 4a and b are DSC and TG curves, respectively. The phase transition temperature of the fluorescent complex is about $149.3\text{ }^\circ\text{C}$, which is much higher than that of $\text{P}(\text{VDF-HFP})$ at $141\text{ }^\circ\text{C}$. Therefore, the doping of the complex can help improve the thermal performance of the nanofiber membrane. Meanwhile, according to the TG-DTA (Thermogravimetry-Differential thermal analysis) curve in Fig. 4b, the complex degrades at $250\text{--}450\text{ }^\circ\text{C}$ for three times, which is consistent with the matrix and ligand of the complex. It was further

Fig. 3 EDS spectra for PFPCFe composite film

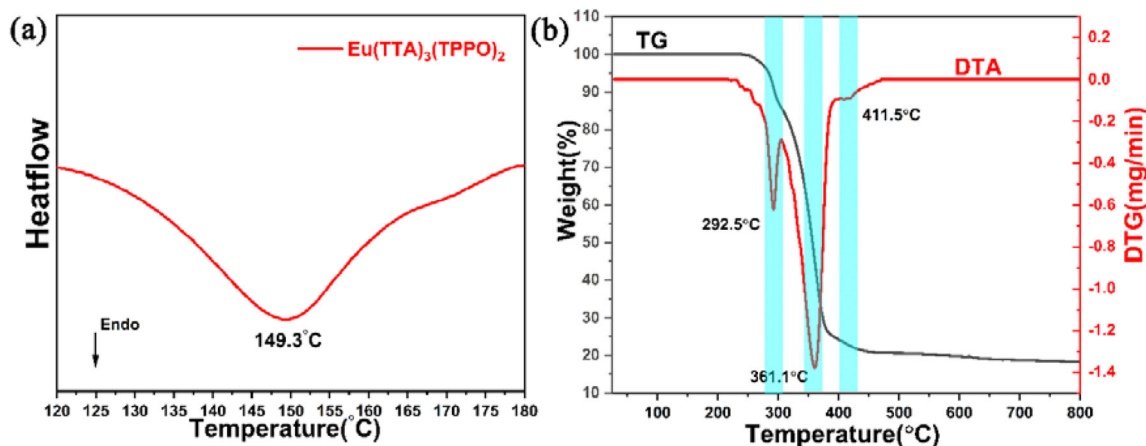
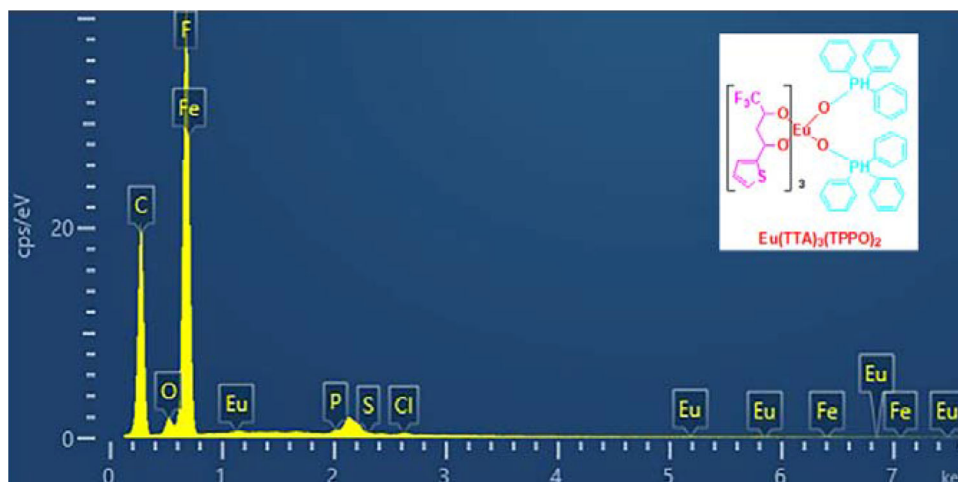


Fig. 4 a DSC and b TG diagram of the complex $\text{Eu}(\text{TTA})_3(\text{TPPO})_2$

confirmed that the complex $\text{Eu}(\text{TTA})_3(\text{TPPO})_2$ was successfully prepared.

3.2 Morphology analysis

The morphology and diameter distribution histogram of electrospun PFP, PFPC, and PFPCFe nanofibers are shown in Fig. 5a–c. It can be seen from the figure of the common random orientation structure, with the increase of feed, the average fiber diameter decreased from 700 to 625 nm and 480 nm. The pores formed by the overlapping of finer nanofibers are smaller than those formed by larger fibers. In addition, with the introduction of additives, the fibers become more evenly distributed, and more excellent electrochemical properties and good mechanical properties can be obtained. This phenomenon may be due to the fact that many functional groups on the surface of filler particles and better

conductivity promote the elongation process of PFP fiber. The EDS-layered image of PFPCFe shown in Fig. 5d–f shows that Eu and Fe elements are evenly distributed, which confirms the success of additive doping and shows that the doped nanoparticles are evenly distributed in the whole fiber.

3.3 XRD and FTIR analyses

As a copolymer of PVDF, P(VDF-HFP) has the same infrared absorption spectrum as PVDF. An identification of absorption bands at 490, 613, 763, 794, 1149, 1209, and 1383 cm^{-1} indicates that these bands are associated with the α -phase and those located at 443, 474, 510, 840, and 1275 cm^{-1} are associated with the β -phase. In the process of study, we mainly take the characteristic peak of α -crystal form as 763 cm^{-1} and β -crystal form as 840 cm^{-1} as the research object. The crystallographic structure of the electrospun PFP,

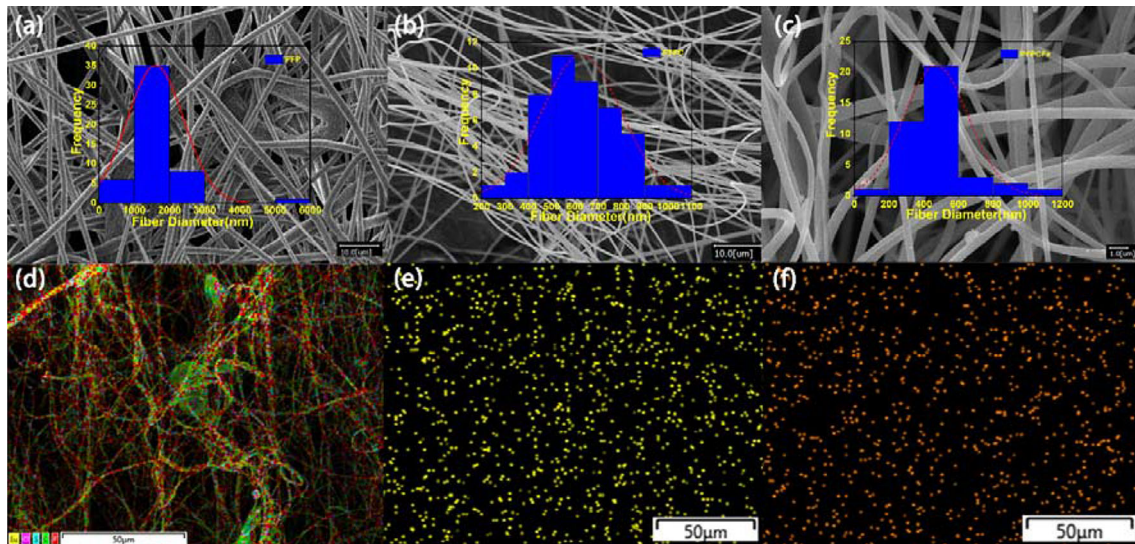


Fig. 5 a–c SEM images of the PFP, PFPC, and PFPCFe, d EDS-layered image of PFPCFe, e–f EDS-layered images of Eu and Fe elements in PFPCFe

PFPC, PFPFe, and PFPCFe nanofiber membranes was characterized by FTIR spectra and XRD patterns. The higher the β -phase content, the better the piezoelectric properties of PVDF fiber [21]. The results of FTIR spectroscopy (Fig. 6b) show that the doping will affect the content of P(VDF-HFP) nanocomposite fibers β -phase formation, in which the simultaneous doping of C and Fe can enhance the maximum ability in the composite fiber β -phase content. The relative fraction of β -phase is calculated by Lambert–Beer law (Eq. 1):

$$F(\beta) = \frac{A_{\beta}}{1.26A_{\alpha} + A_{\beta}} \quad (1)$$

where $F(\beta)$ represents the relative content of β -phase, A_{α} and A_{β} are the corrected heights of characteristic peaks at 763 cm^{-1} and 840 cm^{-1} respectively, that were measured by OMNIC software. Figure 6 shows that in PFPCFe the content of β -phase 96.9% is nearly 20% higher than that of PFP 76.7%, indicating that the addition of additives successfully induced polarity β -phase formation. Figure 7 shows the XRD in the range of 15° – 30° in 2θ , and $2\theta = 18.4^{\circ}$ and 20° correspond to the (020) and (110) crystal planes of the α -phase. Compared with PFP, the sharper diffraction peaks of PFPC, PFPFe, and PFPCFe on the (020) crystal plane and (110) crystal plane are weakened or disappeared. At the same time, a sharper diffraction peak appears at 20.4° ,

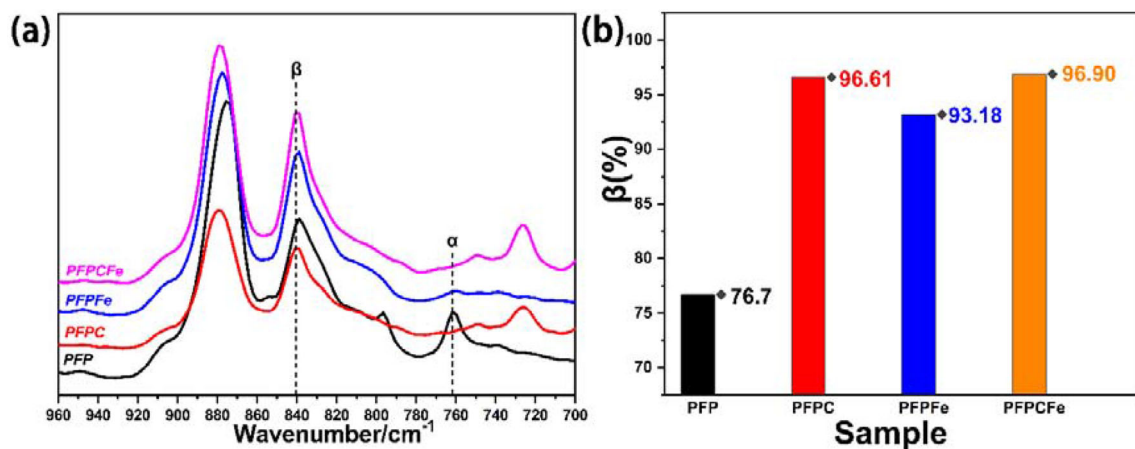


Fig. 6 a FT-IR and b the β -crystal form calculation results of PFP, PFPC, PFPFe, and PFPCFe nanofibers

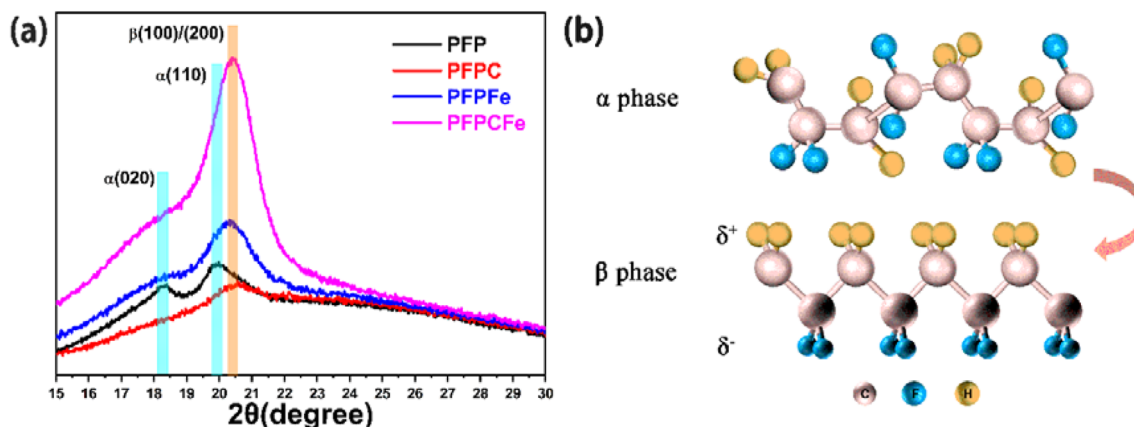


Fig. 7 **a** The β -crystal form calculation results of PFP, PFPC, PFPFe, and PFPCFe nanofibers; **b** β -phase induction mechanism

which corresponds to the β -phase (020) and (110) crystal planes, indicating that the addition of additives promotes the transformation of the α -phase to the β -phase in the P(VDF-HFP) nanocomposite fiber. This conclusion was just consistent with FTIR spectral results. Specifically, this is because the two fillers and the electrospinning process work synergistically to orient the electropositive CH_2 dipole to one side of the PVDF chain (Fig. 7b), inducing the formation of the β -phase [22].

3.4 Atomic force microscopy (AFM) analysis

The AFM images were obtained by MFP-3D Origin (Oxford Instruments Co. USA) using the tips (AC240TS-R3, Asylum) with 2-N/m spring constant and 70-kHz resonance frequency. Phase Retrace represents the lag of the drive signal phase and the sample feedback phase on the tip, the polarization direction of the surface sample, such as domain orientation, shape, size, and distribution. Amplitude Retrace represents the amplitude of the feedback signal, which is used to indicate the magnitude of the polarization and reflect the strength of the piezoelectric signal. In general, can use the Amplitude Retrace and Phase Retrace to compare together to confirm whether the sample has piezoelectricity and the difference in piezoelectric properties in different regions.

We scraped the electrospinning solution of sample PFPCFe for AFM test. Figure 8 shows the domains where the polarization direction is out of plane in the nanofibers. By analyzing them, we can easily see that the polarization direction of PFPCFe has a relatively

uniform distribution out of plane. The surface of the sample is rough and presents a Mongolian yurt roof shaped, and a layered structure appears on the surface, which may be induced by solvent β -phase, β -phase stacking is the reason for this layered fold. It shows that it has a certain piezoelectric response and piezoelectricity. The results are consistent with those of FT-IR (Fig. 3) and XRD (Fig. 4).

3.5 DSC and mechanical stability analyses

The double peak in the DSC results of P(VDF-HFP) polymer is due to its polymorphic structure [23]. FT-IR (Fig. 6) showed that there were α - and β -phase in P(VDF-HFP), corresponding to the endothermic peaks in DSC melting curve (Fig. 9), respectively. As shown in the figure, with the addition of filler, the double peaks became more obvious, and the peaks representing β -phase with the higher crystalline melting temperature (T_m) were dominated. After doping the complex and inorganic filler, the melting peak becomes wider, which may be due to the synergistic effect of filler to rearrange the crystal in P(VDF-HFP), resulting in the formation of β -phase [24]. As can be seen from Table 2, The T_m of PFP is about 141.05 °C and degree of crystallinity (X_c) value is 17.54%, while the T_m of PFPCFe is about 149.94 °C and the X_c is 34.39%. The T_m and X_c values of P(VDF-HFP) were increased by doping the complex and inorganic filler, which is because the T_m of the composite was increased and the crystallization was faster, and the X_c of β -crystal was improved. It also indicates that the doping of the complex and inorganic filler acts as nucleating agent for the β -crystal of

Fig. 8 AFM images of PFPCFe **a** amplitude retrace; **b** phase retrace

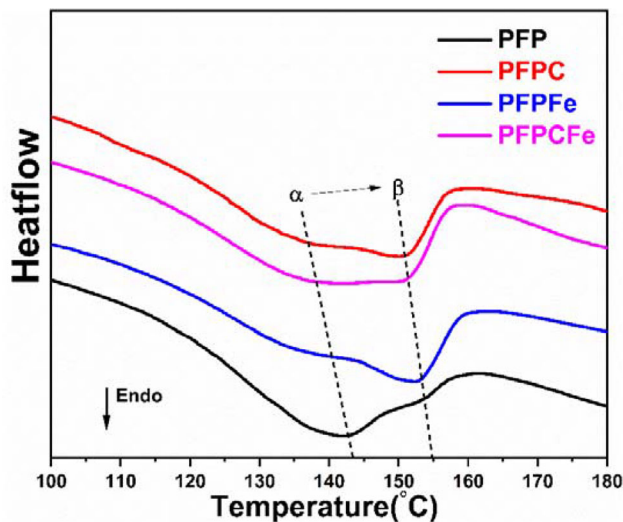
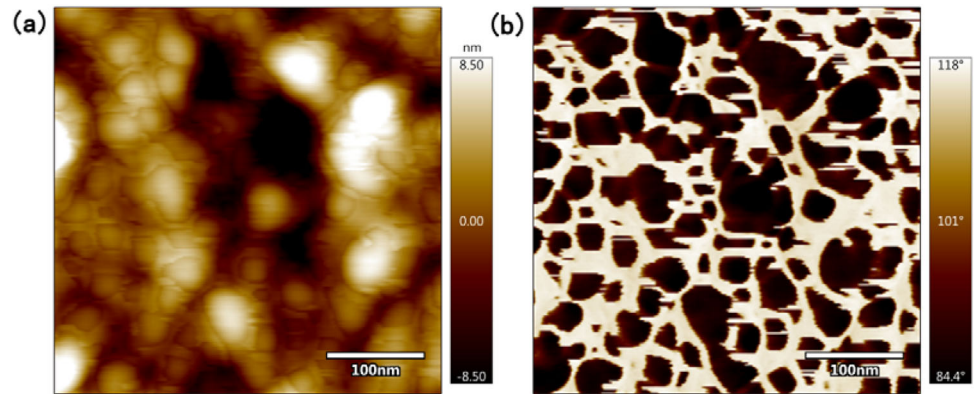


Fig. 9 DSC curves of PFP, PFPC, PFPFe, and PFPCFe nanofibers

Table 2 Melting temperature and degree of crystallinity of PFP, PFPC, PFPFe, and PFPCFe nanofibers

Sample	$T_m/^\circ\text{C}$	$\Delta H_f/(\text{kJ kg}^{-1})$	$X_c/100\%$
PFP	141.05	18.42	17.54
PFPC	150.34	18.71	17.82
PFPFe	152.74	20.83	19.84
PFPCFe	149.94	36.11	34.39

P(VDF-HFP). The DSC results are consistent with those of FT-IR (Fig. 6) and XRD (Fig. 7).

After the sample crystallization melting is determined by DSC, the crystallinity of the sample is calculated by DSC curve, as shown in Eq. (2):

$$X_c = \frac{\Delta H_f}{\Delta H_f^0} \times 100\%, \quad (2)$$

where X_c is the degree of crystallinity, ΔH_f is the melting heat of the crystalline part of the polymer film, ΔH_f^0 is the melting heat of 100% crystallization of the polymer, and ΔH_f^0 of P(VDF-HFP) is 105 J g^{-1} .

Polyurethane elastomer (PU) is a kind of thermoplastic elastomer. The mechanical properties can be greatly improved by spinning PU films on both sides of the sensor functional layer by spinning layer by layer. It can be seen from Fig. 10 that the mechanical properties of the sandwich-structured nanofiber membranes are all greater than that of a single layer. The constructed nanofiber membrane with sandwich structure has relatively high maximum elongation and high tensile strength, while the Young's modulus is reduced. This shows that doped additives will lead to lower crystallinity and small Young's modulus, which is conducive to enhancing the tensile toughness and higher tensile strength of the film. Meanwhile, PU/PFPCFe/PU as a sensor has a strain as high as 230%, making it more suitable for a variety of scenarios.

3.6 Ferroelectric analysis

To study the ferroelectric properties, room-temperature hysteresis loop (P–E) of composite nanofibers and sandwich-structured films is plotted as shown in Fig. 11 at a frequency of 10 Hz. Before performing this experiment, the two sides of the film were coated with copper tape to act as electrodes.

Large hysteresis rings are often observed in normal ferroelectric polymers due to high spontaneous polarization switching, and their normal ferroelectric properties are closely related to crystal structure and morphology. The normal ferroelectric properties of ferroelectric polymers result from high spontaneous

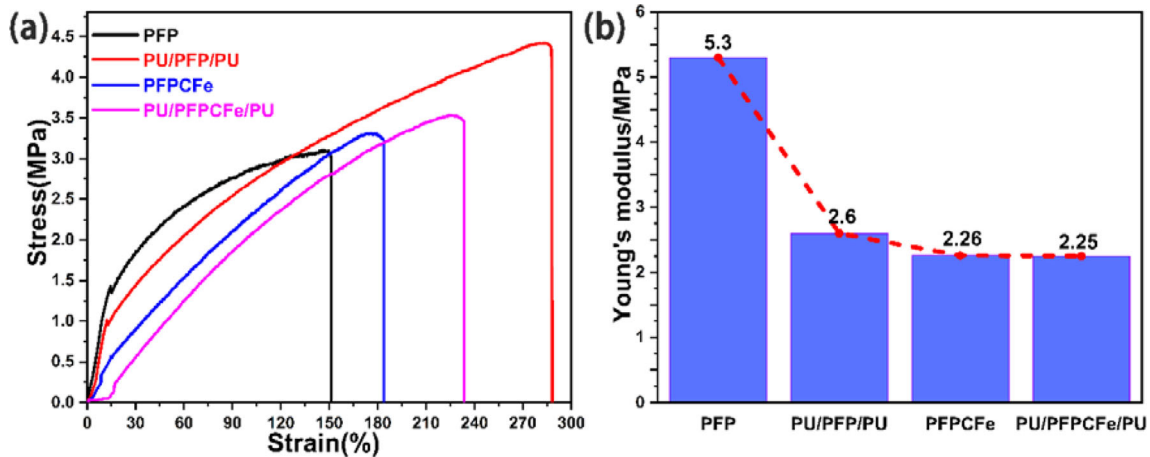


Fig. 10 a Mechanical properties diagram and b Young's modulus diagram of PFP, PU/PFP/PU, PFPCFe, and PU/PFPCFe/PU nanofibers

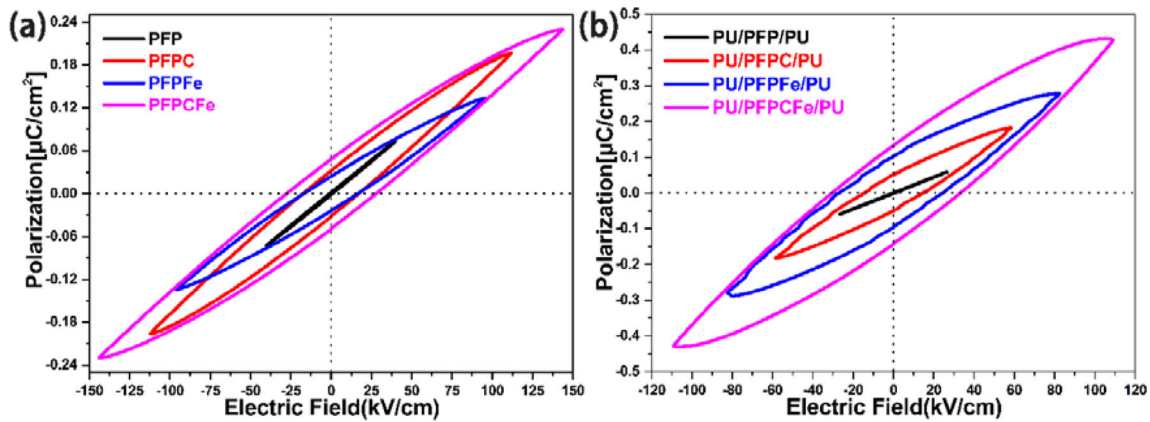


Fig. 11 Room-temperature hysteresis loops (P–E) of a monolayer b sandwich nanofibers

polarization within ferroelectric domains and high compensation polarization or inter-domain coupling outside ferroelectric domains. For pure P(VDF-HFP), the coercive electric field (E_c), the residual polarization value (P_r), and saturated polarization (P_{sat}) values are relatively low (Fig. 11; Table 3), which are 39.8 kV cm^{-1} , $0.002 \text{ } \mu\text{C cm}^{-2}$, and $0.07 \text{ } \mu\text{C cm}^{-2}$, respectively. With the increase of packing concentration, these three values are greatly increased. The E_c of PFPCFe increased by 3.6 times to 143.6 kV cm^{-1} , P_r increased by 25 times to $0.05 \text{ } \mu\text{C cm}^{-2}$, and P_{sat} increased by 3.3 times to $0.23 \text{ } \mu\text{C cm}^{-2}$. Compared with PFPCFe nanofibers, the electric field of sandwich PU/PFPCFe/PU nanofibers decreased slightly, but P_r and P_{sat} increased by 2.8 and 1.8 times, respectively, to $0.14 \text{ } \mu\text{C cm}^{-2}$ and $0.43 \text{ } \mu\text{C cm}^{-2}$. The discharge energy densities (U_e) of PFP, PFPCFe and PU/PFPCFe/PU nanofiber membranes are

calculated according to discharge energy density formula, Eq. (3):

$$U_e = \int_0^{\max} EdD \tag{3}$$

where D is the potential shift, D_{\max} is the potential shift under the highest electric field intensity, and E is the electric field intensity.

The calculated U_e of PFP, PFPCFe and PU/PFPCFe/PU nanofiber membranes are 1.29, 11.14, and 12.52 mJ cm^{-3} , respectively. It can be seen that the filler and sandwich structure can greatly increase the ferroelectric properties of P(VDF-HFP). In β -phase, H and F are arranged in opposite direction giving rise to a nonzero dipole moment responsible for the ferroelectric and piezoelectric properties [25]. The interfacial and space charge effects between filler and matrix improve the polarization of polymer composite system and affect the content of

Table 3 Ferroelectric performance parameters of each sample

Sample	The coercive electric field (E_c) (kV cm ⁻¹)	The remanent polarization (P_r) ($\mu\text{C cm}^{-2}$)	The saturation polarization (P_{sat}) ($\mu\text{C cm}^{-2}$)
PFP	39.8	0.002	0.07
PFPC	95.7	0.003	0.13
PFPCFe	111.7	0.03	0.20
PFPCFe	143.6	0.05	0.23
PU/PFP/PU	26.6	0.001	0.06
PU/PFPC/PU	58.5	0.05	0.18
PU/PFPFe/PU	82.5	0.10	0.28
PU/PFPCFe/PU	109.1	0.14	0.43

electroactive β -phase [26]. The results of ferroelectric properties are consistent with those of FT-IR (Fig. 6), XRD (Fig. 7), and DSC (Fig. 9), which indicates that there is a direct relationship between crystallinity and β -phase enhancement and ferroelectric properties.

3.7 Sensitivity and CIE analysis

A simple 4 cm × 4 cm flexible sensor was fabricated by covering both sides of the prepared nanofiber film with aluminum foil and using wires as electrodes. The most critical parameter of the sensor is the sensitivity, and the sensor sensitivity calculation formula is Eq. (4):

$$S = \frac{\partial \left(\frac{\Delta(C-C_0)}{C_0} \right)}{\partial P}, \quad (4)$$

where C is the output capacitance when pressure P is applied to the sensor and C_0 is the initial output capacitance. As shown in Fig. 12a, we found that by

comparing PFPCFe and PU/PFPCFe/PU sensitivity tests, PU/PFPCFe/PU has a higher sensitivity ($S_1 = 0.29 \text{ kPa}^{-1}$) in the low pressure range (0–5 kPa), which is 3.6 times that of PFPCFe ($S_2 = 0.08 \text{ kPa}^{-1}$). Much higher than the sensitivity values of 0.77% [27], 0.0224 [28], and 0.09 [29] kPa^{-1} are reported in the current literature. It can be found that the sandwich structure can not only improve the mechanical properties of the sensor but also greatly enhance the sensitivity of the sensor.

Figure 12b and Table 4 show the CIE color coordinate diagram. It has relatively close fluorescence characteristics, all of which are the characteristic of red rare earth Eu. Interestingly, the sandwich structure PU/PFPCFe/PU also showed red fluorescence under ultraviolet light, which gave the PU/PFPCFe/PU sensor new performance and more usage scenarios.

Fig. 12 a PFPCFe-based sensor sensitivity comparison; b CIE diagram of C, PFPC, and PFPCFe

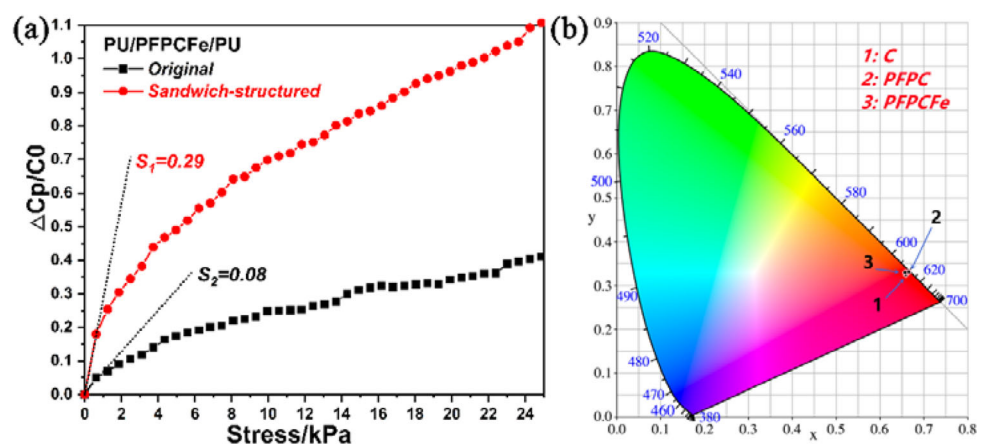


Table 4 CIE values of complex C and nanofibers PFPC and PFPCFe

Point	<i>x</i>	<i>y</i>
1	0.66	0.32
2	0.67	0.33
3	0.66	0.33

3.8 Piezoelectric output performance

Figure 13a shows the structure and working diagram of a simple flexible pressure sensor prepared for us. According to Fig. 13b and c, with the increase of test frequency, the output open-circuit voltage (V_{oc}) and short-circuit current (I_{sc}) increase, and the output of sandwich structure is obviously better than that of single-layer structure. As the frequency increases, the rate of change of the electric dipole moment in the bulk is accelerated, resulting in less charge escaped and more charge accumulated on both surfaces [30]. Under the same area (4 cm × 4 cm) and pressure (12.5 kPa), PU/PFPCFe/PU can achieve a maximum V_{oc} of ~ 3.7 V and I_{sc} of ~ 24 nA at 3 Hz, far exceeding the V_{oc} and I_{sc} of monolayer film under the same conditions. It is also much larger than 15 mV [3] and 300 mV [31] reported in relevant literature. As a device with excellent sensitivity and good piezoelectric output, it can be used in practical

applications, such as health monitoring, pressure detection, signal monitoring, electronic skin sensors, and other fields.

4 Conclusion

In summary, we successfully prepared the rare earth complex $\text{Eu}(\text{TTA})_3(\text{TPPO})_2$, and the study found that Eu^{3+} -doped electrospun luminescent P(VDF-HFP)/ $\text{FeCl}_3 \cdot 6\text{H}_2\text{O}$ nanocomposites can effectively enhance the piezoelectric properties. In this work, the content of β -phase increased by nearly 20–96.9%. The addition of filler significantly increases the content of β -phase of piezoelectric material and improves its piezoelectric properties. The sandwich structure design is helpful to improve the overall properties of the material. The sensor sensitivity of the designed sandwich structure based on PU/PFPCFe/PU nanofiber membrane is improved by 3.6 times to 0.29 kPa^{-1} and piezoelectric output is up to 3.7 V. It has excellent mechanical properties, and the strain can reach 230%. In addition, the addition of fluorescent complex C also gives it good luminescence properties. Due to the above multifunctional advantages, we believe this work would be beneficial to the

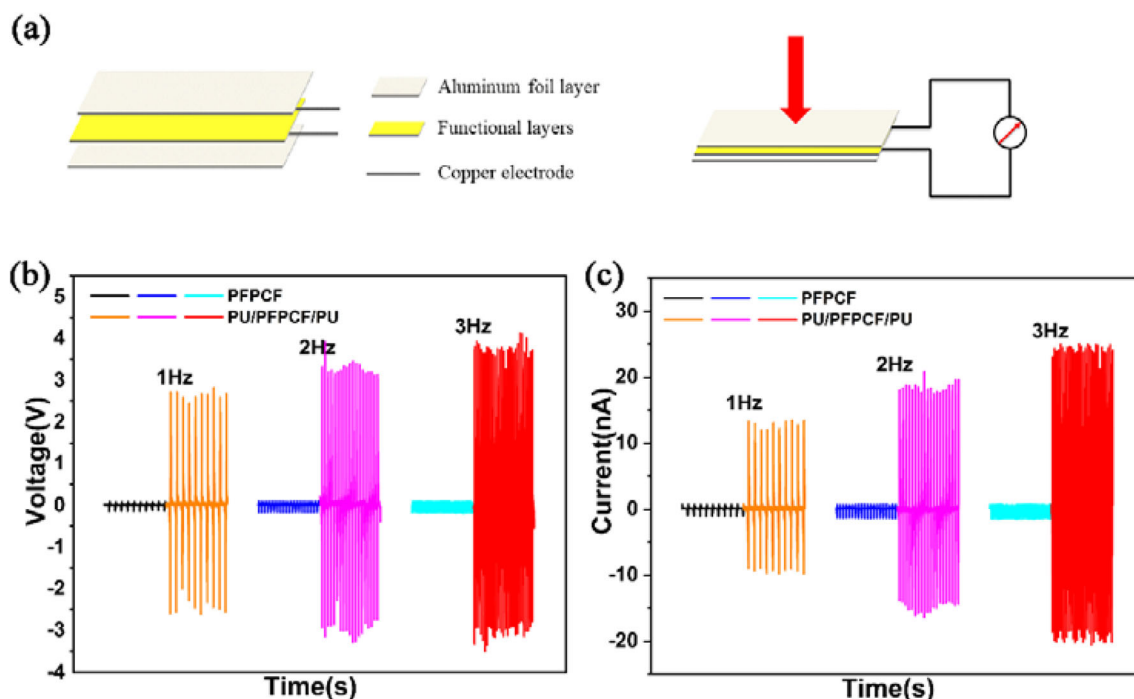


Fig. 13 a Flexible pressure sensor structure and working diagram. b The output open-circuit voltage (V_{oc}) and c short-circuit current (I_{sc}) of the PFPCFe and PU/PFPCFe/PU under different frequencies (1–3 Hz)

development of novel piezoelectric nanofibrous materials that promise applications in wearable electronics, intelligent sensors, and optoelectronic devices. The switching polarity test, load characteristics, power density, stability of piezoelectric device, and applicability on practical fields of our multilayer nanofiber composites are also very important, which is exactly the direction we need to work in future.

Author contributions

GF participated in the data curation, formal analysis, investigation, validation, visualization, and writing of the original draft. YH participated in the data curation and formal analysis. YL contributed to writing, reviewing, & editing of the manuscript. SH participated in the data curation and formal analysis. RX participated in the data curation and formal analysis. YW contributed to writing, reviewing, & editing of the manuscript. WY contributed to writing, reviewing, & editing of the manuscript. QS participated in the supervision, conceptualization, and writing, reviewing, & editing of the manuscript.

Funding

This study was supported by the National Natural Science Foundation of China (No. 52073033), the fund of the Beijing Municipal Education Commission, China (No. 22019821001), and Beijing excellent talent training fund (No. Z2019-042).

Data availability

The datasets generated during and/or analyzed during the current study are available from the corresponding author upon reasonable request.

Declarations

Conflict of interest The authors declare that they have no competing interests.

References

1. Y. Ding, T. Xu, O. Onyilagha, H. Fong, Z. Zhu, Recent advances in flexible and wearable pressure sensors based on

- piezoresistive 3D monolithic conductive sponges. *ACS Appl. Mater. Interfaces* **11**, 6685–6704 (2019)
2. Y. Badali, S. Koçyiğit, A. Aytimur, Ş Altındal, İ Uslu, Synthesis of boron and rare earth stabilized graphene doped poly(vinylidene fluoride) (PVDF) nanocomposite piezoelectric materials. *Polym. Compos.* **40**(9), 3623–3633 (2019)
3. J. Zhao, F. Li, Z. Wang, P. Dong, G. Xia, K. Wang, Flexible PVDF nanogenerator-driven motion sensors for human body motion energy tracking and monitoring. *J. Mater. Sci. Mater. Electron.* **32**(11), 14715–14727 (2021)
4. Y. Guo, J. Xu, W. Wu, S. Liu, J. Zhao, E. Pawlikowska, M. Szafran, F. Gao, Ultralight graphene aerogel/PVDF composites for flexible piezoelectric nanogenerators. *Compos. Commun.* **22**, 100542 (2020)
5. N. Meng, X. Ren, G. Santagiuliana, L. Ventura, H. Zhang, J. Wu, H. Yan, M.J. Reece, E. Bilotti, Ultrahigh β -phase content poly(vinylidene fluoride) with relaxor-like ferroelectricity for high energy density capacitors. *Nat. Commun.* **10**, 4535 (2019)
6. J.E. Trevino, S. Mohan, A.E. Salinas, E. Cueva, K. Lozano, Piezoelectric properties of PVDF-conjugated polymer nanofibers. *J. Appl. Polym. Sci.* **138**(28), 50665 (2021)
7. Y.X. Zhao, Y.J. Chen, G.X. Pan, C. Wang, C.B. Peng, Z.X. Peng, Z.X. Sun, Y.R. Liang, Q.S. Shi, Preparation and performance of novel Tb-PEG + Eu-PEG/PANI/PAN luminescent-electrical-phase change composite fibers by electrospinning. *Chem. J. Chin. Univ. Chin.* **40**(04), 824–831 (2019)
8. C.M. Azzaz, L.H. Mattoso, N.R. Demarquette, R.J. Zednik, Poly(vinylidene fluoride) nanofibers obtained by electrospinning and blowspinning: Electrospinning enhances the piezoelectric β -phase—myth or reality? *J. Appl. Polym. Sci.* **138**(10), 49959 (2021)
9. Z. He, F. Rault, M. Lewandowski, E. Mohsenzadeh, F. Saloun, Electrospun PVDF nanofibers for piezoelectric applications: a review of the influence of electrospinning parameters on the β phase and crystallinity enhancement. *Polymers* **13**, 174 (2021)
10. L. Li, M. Zhang, W. Ruan, Studies on synergistic effect of CNT and CB nanoparticles on PVDF. *Polym. Compos.* **36**(12), 2248–2254 (2015)
11. B. Zheng, J. Fan, B. Chen, X. Qin, J. Wang, F. Wang, X. Liu, Rare-earth doping in nanostructured inorganic materials. *Chem. Rev.* **122**(6), 5519–5603 (2022)
12. V. Varkey, A.R. Chandran, E.T. Jose, I. Paul, G. Jose, Fabrication of photoluminescent electrospun poly(styrene-co-methyl methacrylate) nanofibers integrated with LaPO_4 : Eu^{3+} for optical applications. *Mater. Today: Proc.* **47**, 921–926 (2021)

13. S. Bose, J.R. Summers, B.B. Srivastava, V. Padilla-Gainza, M. Peredo, C.M.T. De Leo, K. Lozano, Efficient near infrared to visible light upconversion from Er/Yb codoped PVDF fibrous mats synthesized using a direct polymer doping technique. *Opt. Mater.* **123**, 111866 (2022)
14. E. Öztürk, E. Karacaoglu, The effect of Eu^{3+} -doping on the photoluminescent properties of REInO_3 (RE = Er, Sm) type phosphors. *Mater. Today Commun.* **25**, 101556 (2020)
15. P. Adhikary, A. Biswas, D. Mandal, Improved sensitivity of wearable nanogenerators made of electrospun Eu^{3+} doped P(VDF-HFP)/graphene composite nanofibers for self-powered voice recognition. *Nanotechnology* **27**, 495501 (2016)
16. Y. Li, M.H. Xu, Y.S. Xia, J.M. Wu, X.K. Sun, S. Wang, G.H. Hu, C.X. Xiong, Multilayer assembly of electrospun/electrosprayed PVDF-based nanofibers and beads with enhanced piezoelectricity and high sensitivity. *Chem. Eng. J.* **388**, 124205 (2020)
17. C. He, H. Wang, L.X. Huang, P. Wang, W. Gao, Study on morphology features and mechanical properties of nanofibers films prepared by different composite electrospinning methods. *Key Eng. Mater.* **841**, 70–75 (2020)
18. H. Cui, Y. Li, X. Zhao, X. Yin, J. Yu, B. Ding, Multilevel porous structured polyvinylidene fluoride/polyurethane fibrous membranes for ultrahigh waterproof and breathable application. *Compos. Commun.* **6**, 63–67 (2017)
19. Q. Gao, B.A.F. Kopera, J. Zhu, X. Liao, C. Gao, M. Retsch, S. Agarwal, A. Greiner, Breathable and flexible polymer membranes with mechanoresponsive electric resistance. *Adv. Funct. Mater.* **30**, 1907555 (2020)
20. G. Fu, Q. Shi, Y. He, L. Xie, Y. Liang, Electroactive and photoluminescence of electrospun P(VDF-HFP) composite nanofibers with Eu^{3+} complex and BaTiO_3 nanoparticles. *Polymer* **240**, 124496 (2021)
21. F. Mokhtari, G.M. Spinks, C. Fay, Z. Cheng, R. Raad, J. Xi, J. Foroughi, Wearable electronic textiles from nanostructured piezoelectric fibers. *Adv. Mater. Technol.* **5**, 1900900 (2020)
22. L. Jin, Y. Zheng, Z.K. Liu, J.S. Li, Y.P.Q. Yi, Y.Y. Fan, L.L. Xu, Y. Li, Enhancement of β -phase crystal content of Poly(vinylidene fluoride) nanofiber web by graphene and electrospinning parameters. *Chin. J. Polym. Sci.* **38**(11), 1239–1247 (2020)
23. C. Merlini, G.M.O. Barra, T.M. Araujo, A. Pegoretti, Electrically pressure sensitive poly(vinylidene fluoride)/polypyrrole electrospun mats. *RSC Adv.* **4**(30), 15749–15758 (2014)
24. M. Khalifa, A. Mahendran, S. Anandhan, Durable, efficient, and flexible piezoelectric nanogenerator from electrospun PANi/HNT/PVDF blend nanocomposite. *Polym. Compos.* **40**(4), 1663–1675 (2019)
25. S. Zhang, W. Tong, J. Wang, W. Wang, Z. Wang, Y. Zhang, Modified sepiolite/PVDF-HFP composite film with enhanced piezoelectric and dielectric properties. *J. Appl. Polym. Sci.* **137**(9), 48412 (2020)
26. S. Mishra, R. Sahoo, L. Unnikrishnan, A. Ramadoss, S. Mohanty, S.K. Nayak, Enhanced structural and dielectric behaviour of PVDF-PLA binary polymeric blend system. *Mater. Today Commun.* **26**, 101958 (2021)
27. H. Shi, M. Al-Rubaiai, C.J. Holbrook, M. Miao, T. Pinto, C. Wang, X. Tan, Screen-printed soft capacitive sensors for spatial mapping of both positive and negative pressures. *Adv. Funct. Mater.* **29**(23), 1809116 (2019)
28. Q. Hua, J. Sun, H. Liu, R. Bao, R. Yu, J. Zhai, Z.L. Wang, Skin-inspired highly stretchable and conformable matrix networks for multifunctional sensing. *Nat. Commun.* **9**, 244 (2018)
29. Z. Lei, P. Wu, Zwitterionic skins with a wide scope of customizable functionalities. *ACS Nano* **12**(12), 12860–12868 (2018)
30. S. Yu, Y. Zhang, Z. Yu, J. Zheng, Y. Wang, H. Zhou, PANi/PVDF-TrFE porous aerogel bulk piezoelectric and triboelectric hybrid nanogenerator based on in-situ doping and liquid nitrogen quenching. *Nano Energy* **80**, 105519 (2021)
31. A. Ahmed, Y. Jia, H. Deb, M.F. Arain, H. Memon, K. Pasha, J. Shao, Ultra-sensitive all organic PVDF-TrFE E-spun nanofibers with enhanced β -phase for piezoelectric response. *J. Mater. Sci. Mater. Electron.* **33**, 3965 (2022)

Publisher's Note Springer Nature remains neutral with regard to jurisdictional claims in published maps and institutional affiliations.

Springer Nature or its licensor holds exclusive rights to this article under a publishing agreement with the author(s) or other rightsholder(s); author self-archiving of the accepted manuscript version of this article is solely governed by the terms of such publishing agreement and applicable law.